ARTICLE

Check for updates

Experimental evidence of Förster energy transfer enhancement in the near field through engineered metamaterial surface waves

Kseniia Lezhennikova [1,2 ✉], Kaizad Rustomji[3,4], Boris T. Kuhlmey [5], Tryfon Antonakakis[2], Pierre Jomin[1], Stanislav Glybovski[6], C. Martijn de Sterke [5], Jérôme Wenger [1 ✉], Redha Abdeddaim[1 ✉] & Stefan Enoch[1]

Plasmonics has been demonstrated to provide fine tuning of the emission properties of single quantum sources (brightness, polarization, directivity, spectrum, lifetime...). However, significantly less is known about the role of surface plasmons in mediating subwavelength Förster resonant energy transfer (FRET) when a second emitter is introduced. Here, we report microwave experiments showing that excitation of surface waves on a dedicated metasurface can strongly mediate FRET in the near-field regime. This work paves the way for metasurfaces engineered to control dipole-dipole energy transfer with applications in lighting sources, photovoltaics, quantum information processing and biophysics.

[1] Aix Marseille Univ, CNRS, Centrale Marseille, Institut Fresnel, Institut Marseille Imaging, AMUTech, 13013 Marseille, France. [2] Multiwave Technologies AG, 3 Chemin du Pré Fleuri, 1228 Geneva, Switzerland. [3] School of Electrical and Computer Engineering and the Ilse Katz Center for Nanoscale Science and Technology, Ben-Gurion University of the Negev, Beer Sheva, Israel. [4] Department of Electrical Engineering and Solid State Institute, Technion – Israel Institute of Technology, Haifa, Israel. [5] Institute for Photonics and Optical Sciences (IPOS), School of Physics, University of Sydney, Sydney, NSW 2006, Australia. [6] School of Physics and Engineering, ITMO University, St. Petersburg, Russia. ✉email: kseniia.lezhennikova@fresnel.fr; jerome.wenger@fresnel.fr; redha.abdeddaim@fresnel.fr

Förster resonance energy transfer (FRET) describes the near-field nonradiative energy transfer between a quantum donor and an acceptor[1]. In the visible range, FRET is the dominant process governing energy transfer for donor–acceptor distances between 3 and 20 nm, and as such, FRET plays a key role in solar light harvesting[2,3], organic lighting sources[4,5], single molecule biophysics[6], and biosensing[7]. FRET is also important in the context of quantum many-body systems[8–10], strong coupling[11–13], and cooperative dipole–dipole interaction[14–16].

For a single quantum emitter, it is well understood that the spontaneous emission can be controlled by the photonic environment via the local density of optical states (LDOS)[17,18]. However, the extension of this concept to the control of the FRET between two emitters (two dipoles) has led to a wide range of observations and seemingly contradictory conclusions between enhancement[19–29], no effect[30–37] or quenching[38–40]. For very short dipole–dipole separations R below $\lambda/100$ (deeply subwavelength), the FRET rate is generally not modified or weakly modified by the photonic environment[21,30,34,36,37]. In contrast, for large R exceeding several wavelengths (far-field regime), the presence of propagating surface plasmon[41–43] or waveguide modes[44,45] can dramatically enhance the coupling of energy between dipoles. However, this is the regime of common radiative energy transfer with a distance dependence of $1/R^2$ in free space, rather than the Förster near-field energy transfer regime with its characteristic distance dependence of $1/R^6$. However, much less is known for intermediate dipole–dipole separations between $\lambda/100$ and $\lambda/2$, corresponding to the near-field regime[46–48]. The direct energy transfer between donor and acceptor for the distance $\lambda/3$ was demonstrated through the use of an optical topological transition (OTT) in a metamaterial[49]. While rich physics is present in this near-field regime, FRET experiments in optics fail to measure the energy transfer rate for separations exceeding 15 nm or $\lambda/40$[27].

Another unanswered question in optics concerns the influence of surface plasmons on FRET. While the theory for absorptionless and dispersion-less media predicts that the FRET rate is unrelated to the LDOS[30,31], the influence of surface plasmons on real metals has not been settled[19,21,24,30,34,42]. Whereas a recent comprehensive theoretical investigation by Cortes and Zubin[50] is consistent with experiments, we report experiments that settle this issue definitively. Experimental demonstrations of this effect are challenging because the required accuracy of controlling the positions and orientation of the donor and acceptor molecules is difficult to achieve.

Here we use the precise control of the experimental conditions available in the microwave domain to investigate the influence of the electromagnetic environment and surface plasmons on FRET in the near-field regime of the emitters (with a separation ranging from $\lambda/20$ to $\lambda/2$). We introduce a dedicated metasurface to support surface waves similar to surface plasmons on metal boundaries in optics but at microwave frequencies[51,52]. The comparison with the perfect electric conductor (PEC) readily shows the influence of the surface waves on near-field FRET. We work in the frequency domain 4–4.5 GHz and all the results are scaled in units of $k_0R = 2\pi R/\lambda$ to provide relevant information and guidelines for the optical domain, where such measurements are not feasible. Our work unambiguously demonstrates the ability of surface waves to enhance FRET in the near-field regime.

Results and discussion
The metasurface design supports TM-polarized surface waves thanks to the square lattice of miniaturized crossed slots cut from a copper sheet with a subwavelength periodicity in both directions[52–54]. The metasurface unit cell, shown in Fig. 1a and b,

is etched in a 20 µm-thick copper film placed over an FR-4 substrate with dielectric permittivity $\varepsilon_r = 4.9 + 0.1i$ as depicted in Fig. 1b. The unit cell has dimensions $a = 8$ mm, $h = 1.9$ mm, $w_1 = 7$ mm, $w_2 = 5$ mm, and $w_3 = 0.5$ mm. This metasurface can be classified as an inductive (aperture-type) frequency-selective surface supporting plasmon-like surface waves at frequencies below 4.5 GHz as shown by the dispersion curve of the first propagating mode (Fig. 1c). The design of the unit cell imposes a Bloch-type surface mode presenting hot spots of the electric and magnetic field at distances smaller than the period from the metallization. In Supplementary Note 1 we discuss the detailed field pattern of the surface wave (calculated using an eigenmode solver) and show that it explains the near-field interaction between a dipole with different orientations with the unit cell. In Supplementary Note 2, we show a close similarity between the frequency-normalized dispersion relations for the metasurface in the microwave regime and silver in the optical regime (Supplementary Fig. 2).

To confirm experimentally the excitation of surface waves on the metasurface by parallel and perpendicular electric dipoles, we use a near-field microprobe (Langer EMV-Technik MFA 01) to map the magnetic field in the vertical plane. The results are shown in (Fig. 1d)[55]. We display the magnetic field in Fig. 1d since it has the best signal-to-noise ratio in our experimental data. Electric and magnetic field maps are compared in Supplementary Note 3. The goal of Fig. 1d is to demonstrate the appearance of surface waves in the presence of the metasurface, compared to the PEC mirror. For both dipole orientations, a surface wave is observed as a field bound to the metasurface far away from the source, in excellent agreement with the numerical simulations. When the metasurface is replaced by a copper plate (equivalent to a perfect electric conductor PEC at microwave frequencies), no surface wave is detected, again in accordance with numerical predictions (Fig. 1d). Altogether, these experimental data demonstrate that surface waves are supported by our metasurface, in close similarity with surface plasmon polaritons in optics[1].

To investigate the dependence of the FRET rate and LDOS as functions of the inter-dipole spacing and their height over the metasurface, the dipoles are connected to a vector network analyzer (VNA, Anritsu model MS2036C and the scattering matrix coefficient S_{12} for two dipoles[22] and coefficient S_{22} with the absence of the acceptor dipole. The same quantities S_{22}^0 and S_{12}^0 are measured when the same dipoles are placed in homogeneous space. The LDOS enhancement with respect to the homogeneous space is defined as[56–58]

$$\frac{\Gamma_D}{\Gamma_D^0} = \frac{\mathrm{Re}(Z_{in})}{\mathrm{Re}(Z_{in}^0)} = \frac{\boldsymbol{n}_D \cdot \mathrm{Im}\left\{\overleftrightarrow{\boldsymbol{G}}(\boldsymbol{r}_D, \boldsymbol{r}_D)\right\} \cdot \boldsymbol{n}_D}{\boldsymbol{n}_D \cdot \mathrm{Im}\left\{\overleftrightarrow{\boldsymbol{G}^0}(\boldsymbol{r}_D, \boldsymbol{r}_D)\right\} \cdot \boldsymbol{n}_D}, \qquad (1)$$

where Z_{in} and Z_{in}^0 are the input impedances of the dipole in the presence of the metasurface and the homogeneous space respectively normalized to a wave impedance of the connected port, defined as

$$\mathrm{Re}(Z_{in}) = \frac{1 - \mathrm{Re}(S_{22})^2 - \mathrm{Im}(S_{22})^2}{[1 - \mathrm{Re}(S_{22})]^2 + \mathrm{Im}(S_{22})^2}. \qquad (2)$$

The FRET rate enhancement factor is given by[21,22]

$$\frac{\Gamma_{DA}}{\Gamma_{DA}^0} = \frac{|Z_{12}|^2}{|Z_{12}^0|^2} = \frac{|S_{12}|^2}{|S_{12}^0|^2} = \frac{\left|\boldsymbol{n}_A \cdot \overleftrightarrow{\boldsymbol{G}}(\boldsymbol{r}_A, \boldsymbol{r}_D) \cdot \boldsymbol{n}_D\right|^2}{\left|\boldsymbol{n}_A \cdot \overleftrightarrow{\boldsymbol{G}^0}(\boldsymbol{r}_A, \boldsymbol{r}_D) \cdot \boldsymbol{n}_D\right|^2}.$$

The dipoles are moved by a programmable 3D positioning system with sub-mm accuracy, corresponding to $\lambda/60$, to reconstruct the dependence of the LDOS and FRET rate enhancement
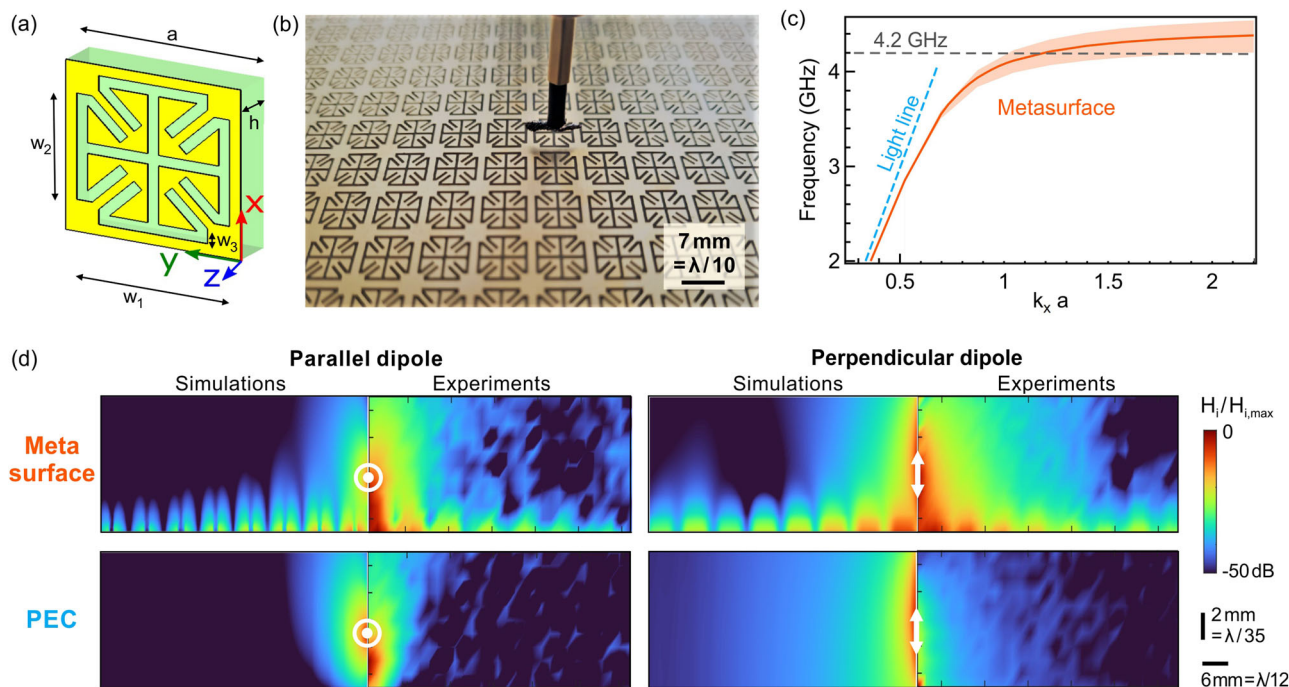
Fig. 1 Metasurface supporting surface waves in the microwave regime and its excitation with a horizontal (parallel) and vertical (perpendicular) dipole. a Illustration of the unit cell ($a = 8$ mm, $h = 1.9$ mm, $w_1 = 7$ mm, $w_2 = 5$ mm, and $w_3 = 0.5$ mm). **b** Photograph of the metasurface and probe used as a dipole source. **c** Dispersion curve of the first propagating surface mode of the metasurface, calculated using the eigenmode solver of CST Microwave Studio 2019. The shaded region indicates the range of deviation due to ±4% variations in the unit cell dimensions (the influence of the dipole's position respective to the metasurface unit cell described in Supplementary Note 1). **d** Simulated and measured magnetic field maps of a parallel and perpendicular dipoles in the presence of the metasurface and near a plane made of perfect electric conductor (PEC), showing that surface waves are excited near the metasurface. The source dipole is located 5 mm ($\lambda/14$) from the mirror. We plot the z component for the parallel dipole and the y component for the perpendicular dipole.

factors with the height z respective to the metasurface plane and the inter-dipole separation R.

We discussed earlier that the relationship between the LDOS and the FRET rate has not been definitively settled[19–40]. Therefore, before discussing our FRET measurements we first present measurements of the evolution of the LDOS enhancement rate with height z to the boundary (Fig. 2a, b). The copper plate (PEC) provides the benchmark to test the validity of the experimental data, as analytical solutions based on the theory are available for this case[17,18]. For both parallel and perpendicular dipole orientations, our experiments are in excellent agreement with the Green function theory. For the parallel dipole, destructive interferences with the dipole mirror image lead to vanishing LDOS in close vicinity to the PEC surface[17], while for the perpendicular dipole, constructive interference enhances the LDOS by a factor of 2. Replacing the copper plate (PEC) with the metasurface introduces a major difference for LDOS at short distances for which $k_0z < 1$ (Fig. 2a, b). Similar to plasmonic metal mirrors in optics[59], the excitation of the surface mode introduces novel energy decay pathways leading to a clear increase of the LDOS for both parallel and perpendicular orientations, in very good agreement with the numerical simulations[17,18]. Our results also show that the surface mode decays quickly in z, such that the source dipole needs to approach the boundary at a distance not larger than $\lambda/6$ ($k_0z < 1$) to excite surface waves.

We now turn to our FRET measurements, showing the evolution of the FRET rate enhancement with the height z to the surface, keeping the dipole-dipole distance constant at $R = \lambda/7$ ($k_0R = 0.9$). For the PEC plate (Fig. 2c), the FRET is quenched for the parallel orientation at short distances to the boundary, in a similar fashion as for the LDOS (Fig. 2a). In contrast, at close

distance to the PEC mirror and for the perpendicular orientation, the theory predicts FRET rate enhancement factors of up to 4 times, since the dipole and its image add up coherently. Due to the finite size of our dipole antennas, our experiments could not approach sufficiently close to the PEC mirror to measure this enhancement in the perpendicular configuration. Otherwise, the PEC results for both orientations are in very good agreement with the theory described in ref. [31] for lossless and weakly dispersive systems. For the metasurface, high FRET enhancements above 10× are reached for both orientations at heights $k_0z < 1$ (Fig. 2d). The presence of surface waves supported by the metasurface radically modifies the energy transfer by opening new dipole–dipole coupling routes in the near-field. This directly highlights the specific role and influence of surface waves in the FRET process.

Finally, we show the FRET enhancement as a function of the dipole–dipole separation R (Fig. 2e, f), keeping the dipole-surface height constant at $z = \lambda/14$ for the parallel orientation and $z = \lambda/10$ for the perpendicular case (due to the finite size of the dipole antennas used in the experiment, we are restricted in the minimum distance to the boundary for the perpendicular orientation). The acceptor dipole is then moved away from the donor dipole, keeping the same orientation and distance to the boundary. For both parallel and perpendicular orientations, the results with the metasurface clearly differ from the PEC case, highlighting again the significant role played by surface waves in mediating the dipole–dipole energy transfer. For a lossless PEC mirror, the FRET rate enhancement at distances ($k_0R > 2$) tends to follow the radiative rate enhancement of the source donor dipole, since for these large k_0R values the energy transfer is dominated by the far-field radiative transfer. For a
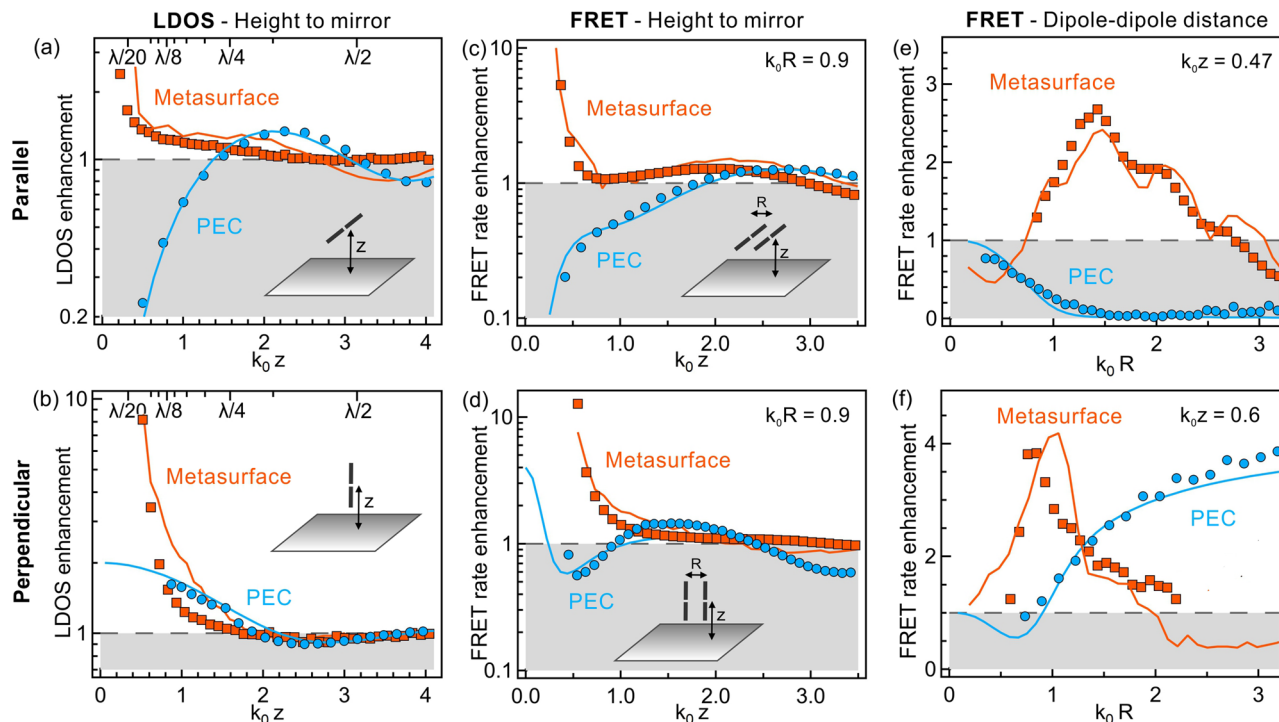
Fig. 2 The influence of surface-wave excitation on the near-field interaction processes between two dipoles. a, b Local density of states (LDOS) enhancement as a function of the height z between the plane of the dipole's center and the boundary plane for parallel (**a**) and perpendicular (**b**) orientation of the dipoles. **c, d** FRET rate enhancement as a function of the height z between the plane of the dipole's center and the boundary plane for the same orientation. The dipole–dipole distance is set at $k_0 R = 0.9$, corresponding to $R = \lambda/7$. **e, f** FRET rate enhancement as a function of the distance R between the two dipoles. For **e**, the height is set at $k_0 z = 0.47$, corresponding to $z = \lambda/14$, while for **f** due to the finite size of the dipoles, we switch to $k_0 z = 0.6$, corresponding to $z = \lambda/10$. In **c, e** both dipoles have parallel orientation to the surface and perpendicular orientation in (**d, f**). In all the graphs, markers correspond to experimental data while lines are numerical calculations. The technical error associated with measurements is described in the "Methods" section.

parallel dipole next to the PEC mirror, the source and its mirror image interfere destructively[17], so the intensity radiated by the donor dipole is quenched, and the FRET rate constant decreases as compared to the free space reference. For the perpendicular case, the source dipole and its mirror image are in phase, resulting in a doubling of the generated field. Therefore, the FRET rate enhancement is around 4 at large $k_0 R$ values.

In the case of the metasurface, the presence of surface waves and nonradiative losses strongly modify this behavior. For the metasurface, we observe FRET enhancement in a specific region of $k_0 R$ between 0.7 and 2.5 corresponding to distances of between $\lambda/9$ and $\lambda/3$. Due to the presence of the discrete unit cells, oscillations are expected as the acceptor is moved away from the source (corresponding to the nodes seen in Fig. 1d)). The numerical simulations also support the oscillations observed at $k_0 R = 1.1, 1.8, 2.5,...$ in Fig. 2e. We find a typical oscillation period of 0.7 which corresponds well with the 8 mm size of the unit cell. The finite size of the dipoles used in our experiment results in averaging of the measured field over their surface, thereby reducing the resolution of the field oscillations in the experimental data. However, the overall trend is still clearly observable.

Having values for both the FRET rate and LDOS enhancement as a function of the distance to the boundary, we can reconsider the data in Fig. 2a–d to study the dependence between FRET and LDOS enhancement factors for both the metasurface and the PEC (Fig. 3). For the PEC plate and perpendicular dipole orientation, the FRET shows no correlation with the LDOS, experimentally confirming the general theory in[31] for absorption-less and dispersion-less media. For the

metasurface, a trend of linear relationship between FRET and LDOS is found for both dipole orientations. In this case, the surface waves play a major role controlling both the LDOS and FRET in the near-field. The surface waves contribute to enhance the donor dipole electric field defining the Green's function which in turn leads to an increase in both the LDOS and the FRET rate[1]. Consequently, an approximately linear relationship between FRET and LDOS appears in the case of the metasurface. This result can be extended to other geometries used in the visible regime like cylindrical metal apertures[24,27,29], plasmonic nanoparticles[23,36,39], and nanoantennas[25,28,37] where surface waves also play a key role. However, for other geometries where surface plasmons have a lesser influence—like a resonant planar cavity for instance— then no direct relationship between FRET and LDOS is to be expected[21,22,33,34,43]. The LDOS depends on the imaginary part of the donor's field at the source position, while the FRET rate depends on the square modulus of the donor's field at the acceptor's position[21,22]. The main difference of the metasurface as compared to PEC or lossless planar cavities is best seen for intermediate donor–acceptor separations with $k_0 R$ around unity. In this case, metasurface waves play a key role in mediating energy transfer. However, for smaller separations $k_0 R < 0.3$, the donor's field at the acceptor position remains essentially unchanged as compared to free space (Fig. 2e, f), so the FRET rate remains unchanged, although the LDOS may still be affected. A comparison of the FRET gains and LDOS found with the metasurface relative to the PEC is shown in Supplementary Note 4 and Supplementary Fig. 4. Our data contribute to solve the long-lasting debate about the FRET–LDOS relationship[19,30] by settling clearly the
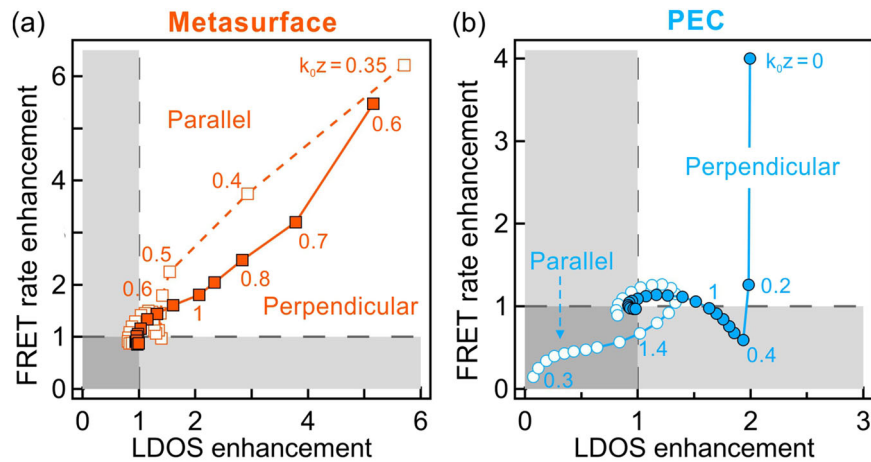
Fig. 3 The LDOS vs. FRET enhancement factors diagrams. The enhancement factor diagrams for the metasurface (**a**), and the plane made of perfect electric conductor (PEC) (**b**). The data corresponds to the experimental results of Fig. 2a–d, with a dipole–dipole distance $R = \lambda/7$. Empty markers connected by dashed lines correspond to parallel dipole orientation, while filled markers and solid lines are for the perpendicular ones. The markers are shown for different heights z to the boundary, the number next to each data point indicates the normalized distance $k_0z = 2\pi z/\lambda$. When the distance z increases, all the curves converge towards the free space (1,1) value.

specific role and influence of the surface waves on planar mirrors.

Conclusion

In conclusion, we have experimentally and numerically shown the strong influence of the excitation of surface waves on both LDOS and FRET. Owing to experimental difficulties in optics, the surface plasmon role was never clearly settled before, leading to a debate among the community[19,21,24,30,34,42]. Here, our data unequivocally demonstrate the strong influence of the surface waves on determining the local enhancement for both LDOS and FRET. The comparison with the PEC case provides direct evidence for the qualitatively different effect of the metasurface and serves as an independent control following Green's function theory. In addition to the deeply subwavelength ($R < \lambda/100$) and the far-field ($R > \lambda$) regimes commonly considered in the literature, our general methodology based on microwave analogy also allows to explore the near-field regime with distances between $\lambda/20$ and $\lambda/2$, which remains challenging to measure directly in optics[27,48]. This work paves the way for new metasurface concepts where the near-field energy transfer is controlled by engineering surface wave propagation in optics, microwaves, and acoustics. The enhanced energy transfer range can benefit various applications to improve light-harvesting photovoltaic devices, quantum many-body interactions studies and biomolecular FRET imaging.

Methods

In both experiments and simulations, we use dipoles with a 10 mm total length, 2 mm width, and a 2 mm gap between the branches. We work in the frequency range from 3 to 5 GHz, thus the dipole resonance frequency remains well outside the frequency range and the dipoles are small enough not to affect the results while still providing enough signal.

Numerical calculations. A numerical model of the full-size sample of the metasurface with a size of 25×25 unit cells (200×200 mm²) and dipole antennas was built in the software CST Microwave Studio 2019. Dipoles were driven by the discreet ports placed in the gap between the branches. For a computation of the LDOS and FRET enhancement, we used a transient solver to obtain scattering parameters.

Fig. 4 Photo of the electric dipoles used in the experiments. The 10 mm dipoles are made from a coaxial cable and fixed on the foam spacer.

Experimental methods. For the experiments, we fabricated the 10 mm dipoles from a coaxial cable of 4 cm length and connected them to a vector network analyzer (VNA, Anritsu model MS2036C) through 1 m coaxial cable for direct measurements of the scattering matrix coefficients S_{11} and S_{21}. The VNA was calibrated over the complete frequency bandwidth considering the presence of the coaxial cables. The two dipoles are held on a foam spacer of $\sim\varepsilon_r \approx 1.08$ dielectric permittivity. Dipoles are shown in Fig. 4. For the measurements of the FRET rate enhancement and LDOS as a function of the height z, two dipoles were fixed at a 10 mm distance from each other, and the center of the plane (copper plane or metasurface) was moved by a programmable 3D positioning system for near-field measurements. For the evaluation of the FRET rate enhancement as a function of the distance R, one of the dipoles was fixed on the plane and the second one is moved by a 3D positioning system away from the first dipole and parallel to the plane.

The smallest measured values of the transmission coefficient for such small dipoles are up to $5*10^{-3}$ for the parallel dipole orientation. For the perpendicular case we used the spatialized electric field probe was used (MVG SAR PROBE SN 17/21 EP353) since the signal power is even lower and it was up to $3*10^{-8}$ V. A technical error associated with VNA measurement is around $3*10^{-4}$ and for the electric field probe is around $1*10^{-9}$ V, which is smaller than the data points on the graphs and does not affect the FRET rate enhancement calculations. We note that we performed direct individual measurements,

and no statistical analysis was done in this work, thus statistical or systematic error analysis is not applicable. The highest measured values for the LDOS near the Metasurfaces are at $f = 4.23$ GHz and $f = 3.98$ GHz for the parallel and perpendicular orientations, respectively. The corresponding simulation results are $f = 4.32$ GHz and $f = 4.22$ GHz, respectively. The difference between the numerical simulations and experiments is likely to be due to inaccuracy in the etching dimensions of the unit cell (the limit of the manufacturing corresponding to an uncertainty of the unit cell dimensions of about 4%). These measurements are highly sensitive to the dipole position on the unit cell, the position of the cables and the position of the second dipole. All the experiments reported here are performed at these frequencies.

References

1. L. Novotny and B. Hecht, *Principles of Nano-Optics* (Cambridge University Press, 2012).
2. Scholes, G. D. Long-range resonance energy transfer in molecular systems. *Annu. Rev. Phys. Chem.* **54**, 57 (2003).
3. Hardin, B. E. et al. Increased light harvesting in dye-sensitized solar cells with energy relay dyes. *Nat. Photonics* **3**, 406 (2009).
4. Baldo, M. A., Thompson, M. E. & Forrest, S. R. High-efficiency fluorescent organic light-emitting devices using a phosphorescent sensitizer. *Nature* **403**, 750 (2000).
5. D'Andrade, B. W. & Forrest, S. R. White organic light-emitting devices for solid-state lighting. *Adv. Mater.* **16**, 1585 (2004).
6. Lerner, E. et al. Toward dynamic structural biology: two decades of single-molecule förster resonance energy transfer. *Science* **359**, eaan1133 (2018).
7. Medintz, I. L. et al. Self-assembled nanoscale biosensors based on quantum Dot FRET donors. *Nat. Mater.* **2**, 630 (2003).
8. Landig, R. et al. Quantum phases from competing short- and long-range interactions in an optical lattice. *Nature* **532**, 7600 (2016).
9. Bluvstein, D. et al. Controlling quantum many-body dynamics in driven Rydberg atom arrays. *Science* **371**, 1355 (2021).
10. Osterloh, K., Barberán, N. & Lewenstein, M. Strongly correlated states of ultracold rotating dipolar fermi gases. *Phys. Rev. Lett.* **99**, 160403 (2007).
11. Coles, D. M. et al. Polariton-mediated energy transfer between organic dyes in a strongly coupled optical microcavity. *Nat. Mater.* **13**, 712 (2014).
12. Zhong, X. et al. Non-radiative energy transfer mediated by hybrid light-matter states. *Angew. Chem. Int. Ed.* **55**, 6202 (2016).
13. Garcia-Vidal, F. J. & Feist, J. Long-distance operator for energy transfer. *Science* **357**, 1357 (2017).
14. Cortes, C. L. & Jacob, Z. Super-coulombic atom–atom interactions in hyperbolic media. *Nat. Commun.* **8**, 1 (2017).
15. Keaveney, J. et al. Cooperative Lamb shift in an atomic vapor layer of nanometer thickness. *Phys. Rev. Lett.* **108**, 173601 (2012).
16. Pustovit, V. N. & Shahbazyan, T. V. Cooperative emission of light by an ensemble of dipoles near a metal nanoparticle: the plasmonic Dicke effect. *Phys. Rev. Lett.* **102**, 077401 (2009).
17. Barnes, W. L., Horsley, S. A. R. & Vos, W. L. Classical antennas, quantum emitters, and densities of optical states. *J. Opt.* **22**, 073501 (2020).
18. Carminati, R. et al. Electromagnetic density of states in complex plasmonic systems. *Surf. Sci. Rep.* **70**, 1 (2015).
19. Andrew, P. & Barnes, W. L. Förster energy transfer in an optical microcavity. *Science* **290**, 785 (2000).
20. Hopmeier, M., Guss, W., Deussen, M., Göbel, E. O. & Mahrt, R. F. Enhanced dipole–dipole interaction in a polymer microcavity. *Phys. Rev. Lett.* **82**, 4118 (1999).
21. Rustomji, K. et al. Direct imaging of the energy-transfer enhancement between two dipoles in a photonic cavity. *Phys. Rev. X* **9**, 011041 (2019).
22. Rustomji, K. et al. Complete electromagnetic dyadic green function characterization in a complex environment—resonant dipole–dipole interaction and cooperative effects. *Phys. Rev. X* **11**, 021004 (2021).
23. Aissaoui, N. et al. FRET enhancement close to gold nanoparticles positioned in DNA origami constructs. *Nanoscale* **9**, 673 (2017).
24. Ghenuche, P., de Torres, J., Moparthi, S. B., Grigoriev, V. & Wenger, J. Nanophotonic enhancement of the förster resonance energy-transfer rate with single nanoapertures. *Nano Lett.* **14**, 4707 (2014).
25. Bidault, S. et al. Competition between Förster resonance energy transfer and donor photodynamics in plasmonic dimer nanoantennas. *ACS Photonics* **3**, 895 (2016).
26. de Torres, J. et al. Plasmonic nanoantennas enable forbidden Förster Dipole–Dipole energy transfer and enhance the FRET efficiency. *Nano Lett.* **16**, 6222 (2016).
27. Baibakov, M. et al. Extending single-molecule förster resonance energy transfer (FRET) range beyond 10 nanometers in zero-mode waveguides. *ACS Nano* **13**, 8469 (2019).
28. Hamza, A. O., Viscomi, F. N., Bouillard, J.-S. G. & Adawi, A. M. Förster resonance energy transfer and the local optical density of states in plasmonic nanogaps. *J. Phys. Chem. Lett.* **12**, 1507 (2021).
29. Patra, S., Claude, J.-B. & Wenger, J. Fluorescence brightness, photostability, and energy transfer enhancement of immobilized single molecules in zero-mode waveguide nanoapertures. *ACS Photonics* (2022).
30. Blum, C. et al. Nanophotonic control of the förster resonance energy transfer efficiency. *Phys. Rev. Lett.* **109**, 203601 (2012).
31. Wubs, M. & Vos, W. L. Förster resonance energy transfer rate in any dielectric nanophotonic medium with weak dispersion. *N. J. Phys.* **18**, 053037 (2016).
32. Rabouw, F. T., den Hartog, S. A., Senden, T. & Meijerink, A. Photonic effects on the förster resonance energy transfer efficiency. *Nat. Commun.* **5**, 3610 (2014).
33. Schleifenbaum, F., Kern, A. M., Konrad, A. & Meixner, A. J. Dynamic control of förster energy transfer in a photonic environment. *Phys. Chem. Chem. Phys.* **16**, 12812 (2014).
34. Konrad, A., Metzger, M., Kern, A. M., Brecht, M. & Meixner, A. J. Controlling the dynamics of Förster resonance energy transfer inside a tunable sub-wavelength Fabry–Pérot-resonator. *Nanoscale* **7**, 10204 (2015).
35. Roth, D. J. et al. Förster resonance energy transfer inside hyperbolic metamaterials. *ACS Photonics* **5**, 4594 (2018).
36. Bohlen, J. et al. Plasmon-assisted Förster resonance energy transfer at the single-molecule level in the moderate quenching regime. *Nanoscale* **11**, 7674 (2019).
37. Sanz-Paz, M., Wenger, J., van Hulst, N. F., Mivelle, M. & Garcia-Parajo, M. F. Nanoscale control of single molecule Förster resonance energy transfer by a scanning photonic nanoantenna. *Nanophotonics* **9**, 4021 (2020).
38. Weeraddana, D., Premaratne, M., Gunapala, S. D. & Andrews, D. L. Controlling resonance energy transfer in nanostructure emitters by positioning near a mirror. *J. Chem. Phys.* **147**, 074117 (2017).
39. Jeong, Y. & Schatz, G. C. Enhancement and suppression of resonance energy transfer near metal nanoparticles. *J. Phys. Chem. C* **124**, 20589 (2020).
40. Collison, R. et al. Purcell effect of plasmonic surface lattice resonances and its influence on energy transfer. *ACS Photonics* **8**, 2211 (2021).
41. Bouchet, D. et al. Long-range plasmon-assisted energy transfer between fluorescent emitters. *Phys. Rev. Lett.* **116**, 037401 (2016).
42. Wu, J.-S., Lin, Y.-C., Sheu, Y.-L. & Hsu, L.-Y. Characteristic distance of resonance energy transfer coupled with surface plasmon polaritons. *J. Phys. Chem. Lett.* **9**, 7032 (2018).
43. Wei, Y.-C. et al. Can nanocavities significantly enhance resonance energy transfer in a single donor–acceptor pair? *J. Phys. Chem. C* **125**, 18119 (2021).
44. de Roque, P. M., van Hulst, N. F. & Sapienza, R. Nanophotonic boost of intermolecular energy transfer. *N. J. Phys.* **17**, 113052 (2015).
45. de Torres, J., Ferrand, P., Colas des Francs, G. & Wenger, J. Coupling emitters and silver nanowires to achieve long-range plasmon-mediated fluorescence energy transfer. *ACS Nano* **10**, 3968 (2016).
46. Andrew, P. & Barnes, W. L. Energy transfer across a metal film mediated by surface plasmon polaritons. *Science* **306**, 1002 (2004).
47. Newman, W. D. et al. Observation of long-range dipole-dipole interactions in hyperbolic metamaterials. *Sci. Adv.* **4**, eaar5278 (2018).
48. Boddeti, A. K. et al. Long-range dipole–dipole interactions in a plasmonic lattice. *Nano Lett.* **22**, 22 (2022).
49. Deshmukh, R. et al. Long-range resonant energy transfer using optical topological transitions in metamaterials. *ACS Photonics* **5**, 2737 (2018).
50. Cortes, C. L. & Jacob, Z. Fundamental figures of merit for engineering förster resonance energy transfer. *Opt. Express* **26**, 19371 (2018).
51. Pendry, J. B., Martín-Moreno, L. & Garcia-Vidal, F. J. Mimicking surface plasmons with structured surfaces. *Science* **305**, 847 (2004).
52. Glybovski, S. B., Tretyakov, S. A., Belov, P. A., Kivshar, Y. S. & Simovski, C. R. Metasurfaces: from microwaves to visible. *Phys. Rep.* **634**, 1 (2016).
53. Anderson, I. On the Theory of Self-Resonant Grids. *Bell Syst. Tech. J.* **54**, 1725 (1975).
54. Luukkonen, O. et al. Simple and accurate analytical model of planar grids and high-impedance surfaces comprising metal strips or patches. *IEEE Trans. Antennas Propag.* **56**, 1624 (2008).
55. Baraclough, M., Hooper, I. R. & Barnes, W. L. Metamaterial analogues of strongly coupled molecular ensembles. *ACS Photonics* **8**, 2997 (2021).
56. Greffet, J.-J., Laroche, M. & Marquier, F. Impedance of a nanoantenna and a single quantum emitter. *Phys. Rev. Lett.* **105**, 117701 (2010).

57. Krasnok, A. E. et al. An antenna model for the Purcell effect. *Sci. Rep.* **5**, 12956 (2015).
58. Rustomji, K., Abdeddaim, R., de Sterke, C. M., Kuhlmey, B. & Enoch, S. Measurement and simulation of the polarization-dependent Purcell factor in a microwave fishnet metamaterial. *Phys. Rev. B* **95**, 035156 (2017).
59. Chizhik, A. I., Rother, J., Gregor, I., Janshoff, A. & Enderlein, J. Metal-induced energy transfer for live cell nanoscopy. *Nat. Photonics* **8**, 124 (2014).

Author contributions

L.K. performed the calculations, L.K. and P.J. performed the experiments, J.W., S.E., R.A., T.A. conceived the research, J.W., S.E., R.A., S.G., C.M.d.S., and T.A. supervised the study. L.K. wrote the first draft. K.R., B.T.K., J.W., S.E., R.A., S.G., and C.M.d.S. discussed the results and physical interpretation and wrote the final version of the manuscript.

Competing interests

The authors declare no competing interests.

Additional information

Supplementary information The online version contains supplementary material available at https://doi.org/10.1038/s42005-023-01347-1.

Correspondence and requests for materials should be addressed to Kseniia Lezhennikova, Jérôme Wenger or Redha Abdeddaim.

Peer review information *Communications Physics* thanks the anonymous reviewers for their contribution to the peer review of this work.

Reprints and permission information is available at http://www.nature.com/reprints

Publisher's note Springer Nature remains neutral with regard to jurisdictional claims in published maps and institutional affiliations.